

Wave propagation in an elastic lattice with non-reciprocal stiffness and engineered damping

Harshit Kumar Sandhu,¹ Saurav Dutta,¹ and Rajesh Chaunsali^{1, a)}

Department of Aerospace Engineering, Indian Institute of Science, Bangalore 560012, India

(Dated: 1 August 2025)

Nonreciprocal wave propagation allows for directional energy transport. In this work, we systematically investigate wave dynamics in an elastic lattice that combines nonreciprocal stiffness with viscous damping. After establishing how conventional damping counteracts the system's gain, we introduce a non-dissipative form of nonreciprocal damping in the form of gyroscopic damping. We find that the coexistence of nonreciprocal stiffness and nonreciprocal damping results in a decoupled control mechanism. The nonreciprocal stiffness is shown to govern the temporal amplification rate, while the nonreciprocal damper independently tunes the wave's group velocity and oscillation frequency. This decoupling gives rise to phenomena such as the enhancement of net amplification for slower-propagating waves and boundary-induced wave mixing. These findings provide a theoretical framework for designing active metamaterials with more versatile control over their wave propagation characteristics.

I. INTRODUCTION

The ability to control the flow of wave energy is a central theme in physics and engineering. Systems that break reciprocity—the symmetry of transmission between a source and a receiver—enable unique wave phenomena and have led to applications such as acoustic diodes, unidirectional amplifiers, and robust vibration isolators (Nassar *et al.*, 2020). A common method to achieve nonreciprocity is to engineer asymmetric couplings in a lattice, an idea rooted in the Hatano-Nelson model (Hatano and Nelson, 1996; 1998). This approach creates active systems where waves are amplified in one direction while being attenuated in the opposite (Brandenbourger *et al.*, 2019). This concept has more recently been placed within the broader context of non-Hermitian topology (Shen *et al.*, 2018; Yao and Wang, 2018), which connects nonreciprocal couplings to the non-Hermitian skin effect—the localization of bulk modes at a system's boundaries (Ding *et al.*, 2022; Lin *et al.*, 2023).

The physical realization of these models often relies on active feedback control, where sensors and actuators generate direction-dependent interaction forces. Such nonreciprocal couplings have been demonstrated on various platforms, including acoustic (Maddi *et al.*, 2024; Zhang *et al.*, 2021), mechanical (Brandenbourger *et al.*, 2019; Ghatak *et al.*, 2020; Wang *et al.*, 2022), and electric lattices (Jana *et al.*, 2025; Liu *et al.*, 2021). Since momentum is locally injected by each element to amplify bulk waves in a preferential direction, these lattices are distinct from momentum-conserving “odd elastic” solids (Banerjee *et al.*, 2021; Chen *et al.*, 2021; Gao *et al.*, 2022; Scheibner *et al.*, 2020; Zhao *et al.*, 2020).

Despite these advances, research has predominantly focused on nonreciprocal stiffness, where interaction

forces are proportional to relative displacements (Brandenbourger *et al.*, 2019; Rosa and Ruzzene, 2020). In this context, damping is generally treated as a parasitic effect that simply counteracts the system's gain. This perspective, however, overlooks the possibility of engineering damping itself as a functional tool for wave manipulation.

In this paper, we explore this possibility by introducing a nonreciprocal damping mechanism into a lattice with nonreciprocal stiffness. We demonstrate that this interplay gives rise to a decoupled control mechanism. Specifically, we show that the nonreciprocal stiffness governs the wave's temporal amplification rate, while the nonreciprocal damping (gyroscopic damping (Carta *et al.*, 2014)) term independently tunes its group velocity and oscillation frequency. This decoupling offers a more versatile method for controlling wave propagation in active media than is achievable with nonreciprocal stiffness alone.

The paper is organized as follows. Section II reviews the model with nonreciprocal stiffness and analyzes its interaction with conventional damping. In Sec. III, we introduce a specialized, non-dissipative, nonreciprocal damper and examine its isolated effect on wave propagation. The full system combining both types of nonreciprocity is investigated in Sec. IV, where we detail the decoupled control mechanism and its consequences, such as boundary-induced wave mixing. Finally, Sec. V summarizes our findings and concludes the paper.

II. LATTICE WITH NONRECIPROCAL STIFFNESS

We consider a one-dimensional elastic lattice as illustrated in Fig. 1(a). Each unit cell contains a point mass m , attached to an onsite (ground) spring of stiffness k_g , and coupled to neighboring masses via nonreciprocal intersite springs. The stiffness in the forward direction is $k_f = k(1 + \alpha)$, and in the backward direction

^{a)}Email: rchaunsali@iisc.ac.in

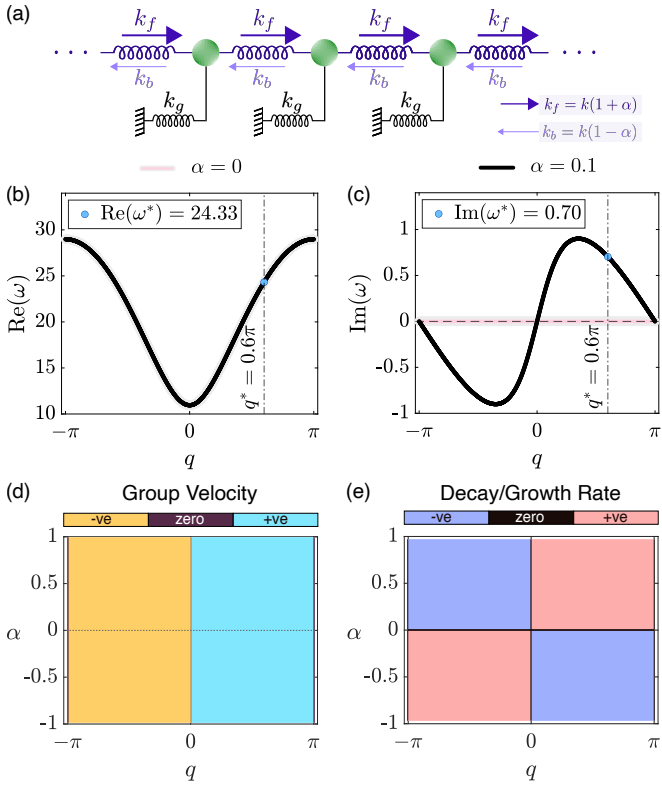


FIG. 1. Wave propagation in a 1D lattice with nonreciprocal stiffness. (a) Schematic of the lattice with asymmetric intersite springs characterized by forward and backward stiffnesses $k_f = k(1 + \alpha)$ and $k_b = k(1 - \alpha)$. (b–c) Real and imaginary parts of the complex dispersion relation $\omega(q)$ for asymmetry parameter $\alpha = 0$ and $\alpha = 0.1$. (d–e) Parametric maps of group velocity and decay/growth rate signs as functions of wavenumber q and asymmetry α , highlighting directional energy transport in the absence of damping. We take intersite stiffness $k = 180$, onsite stiffness $k_g = 120$, and mass $m = 1$ in these calculations.

is $k_b = k(1 - \alpha)$, where $\alpha \in [-1, 1]$ quantifies the degree of nonreciprocity.

In the following subsections, we analyze wave propagation characteristics in such lattices, beginning with the undamped case and subsequently incorporating the effects of viscous damping.

A. No damper

We first revisit the lattice without any damper, which has been addressed in several prior studies (Brandenbourger *et al.*, 2019). The equation of motion for the displacement $u_n(t)$ of the n th mass is given by

$$m\ddot{u}_n + (2k + k_g)u_n - k(1 + \alpha)u_{n-1} - k(1 - \alpha)u_{n+1} = 0. \quad (1)$$

To analyze wave propagation, we employ the Bloch-Floquet ansatz $u_n(t) = \hat{u}e^{i(qn - \omega t)}$, where \hat{u} is the amplitude, q is the wavenumber, and ω is the angular frequency. Substituting into the equation of motion yields

the dispersion relation:

$$\omega(q) = \sqrt{\frac{1}{m} [k_g + 2k(1 - \cos q) + 2ik\alpha \sin q]}. \quad (2)$$

For $\alpha \neq 0$, the dispersion relation yields complex-valued ω for real q . This implies both temporal oscillations, captured by $\text{Re}[\omega(q)]$, and temporal growth or decay, governed by $\text{Im}[\omega(q)]$. The real and imaginary components can be expressed as

$$\text{Re}[\omega(q)] = \sqrt{r(q)} \cos\left(\frac{\theta(q)}{2}\right), \quad (3)$$

$$\text{Im}[\omega(q)] = \sqrt{r(q)} \sin\left(\frac{\theta(q)}{2}\right), \quad (4)$$

where the auxiliary quantities are defined as

$$r(q) = \sqrt{A(q)^2 + B(q)^2}, \quad \theta(q) = \text{atan2}(B(q), A(q)),$$

$$A(q) = \frac{1}{m} [k_g + 2k(1 - \cos q)], \quad B(q) = \frac{2k\alpha \sin q}{m}.$$

Figures 1(b) and 1(c) show the real and imaginary parts of the dispersion relation for $\alpha = 0.1$, alongside the reciprocal case ($\alpha = 0$) for comparison. The real part, $\text{Re}[\omega(q)]$, exhibits negligible variation, whereas the imaginary part, $\text{Im}[\omega(q)]$, reveals significant nonreciprocal behavior: attenuation for $q < 0$ and amplification for $q > 0$. These behaviors become clearer in the small- α limit, where the dispersion relation admits the following approximations:

$$\text{Re}[\omega(q)] = \sqrt{A(q)} + \frac{k^2 \alpha^2 \sin^2 q}{2m^2 A(q)^{3/2}} + \mathcal{O}(\alpha^3), \quad (5)$$

$$\text{Im}[\omega(q)] = \frac{k\alpha \sin q}{m\sqrt{A(q)}} + \mathcal{O}(\alpha^3). \quad (6)$$

These expressions reveal that the leading-order correction appears exclusively in the imaginary part of the complex frequency, $\text{Im}[\omega(q)]$. Consequently, this term has a dominant effect on the temporal amplification or decay of the wave, while the corresponding correction to the real part of the frequency is of a higher order. It is noteworthy, however, that this small correction results in an *increase* in the oscillation frequency, a behavior opposite to that reported in some recently studied systems (Rosa and Ruzzene, 2020). Furthermore, for a fixed value of α , the sign of $\text{Im}[\omega(q)]$ is determined by the sign of the wave number q .

We also observe that $\text{Re}[\omega(q)]$ is symmetric about $q = 0$, while $\text{Im}[\omega(q)]$ is antisymmetric. This property holds for all values of α , as $r(q)$ is an even function and $\theta(q)$ is an odd function of q , thereby imparting the observed symmetry properties to the dispersion relations in Eqs. (3) and (4).

These observations imply that a wave packet centered at a particular frequency will travel symmetrically in both directions with identical group velocities, given

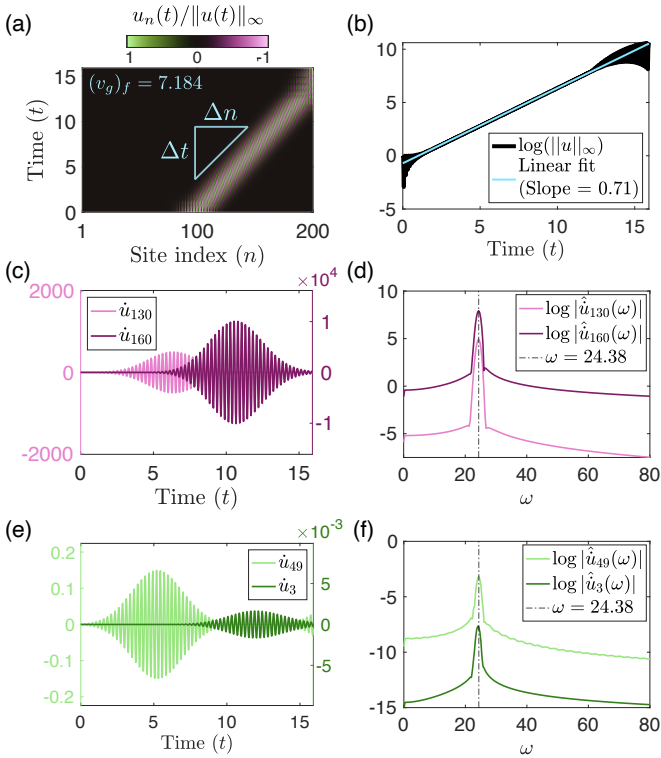


FIG. 2. Numerical demonstration of directional wave amplification in a 1D lattice with nonreciprocal stiffness. (a) Space-time colormap of the normalized displacement field in a finite lattice of 200 particles with fixed boundaries, showing pronounced amplification in the forward-propagating wave packet. The observed group velocity is $v_g \approx 7.184$. (b) Logarithmic plot of the instantaneous global maximum of the lattice displacement field, with a linear fit yielding a slope of 0.71. (c-d) Velocity responses and corresponding spectral amplitudes at downstream sites ($n = 130, 160$) highlight energy amplification and dominant excitation near $\omega \approx 24.38$ rad/s. (e-f) Upstream sites ($n = 49, 3$) exhibit strong attenuation in both time and frequency domains, confirming unidirectional energy transport enabled by non-reciprocal stiffness.

by $\frac{d}{dq} \text{Re}[\omega(q)]$, while undergoing asymmetric amplification or decay. Figures 1(d) and 1(e) present parametric plots showing the sign of the group velocity and the amplification/decay rates as functions of α . The group velocity maintains its sign across all values of α , with zeros at $q = 0, \pm\pi$. The growth/decay map indicates that amplification occurs when α and q share the same sign. Reversing the sign of α reverses the direction of amplification.

Next, we perform numerical simulations and verify the nonreciprocal wave propagation in a finite lattice setting shown in Fig. 2. We take a 200-particle chain with fixed boundary conditions and provide an initial condition in the middle of the chain in the form of a Gaussian-modulated wave packet centered at $|q^*| = 0.6\pi$, corresponding to a temporal growth [marked in Fig. 1(c)]. The

prescribed initial displacement (with vanishing velocity) of the n th particle is given by

$$u_n(0) = \exp\left[-\frac{(n - n_0)^2}{2\sigma^2}\right] \cos(q^*n),$$

where $n_0 = 100$ is the center of the excitation, and $\sigma = 12$ is the envelope width.

Figure 2(a) shows the space-time evolution of the normalized displacement field, $u_n(t)/\|u(t)\|_\infty$, where $\|u(t)\|_\infty = \max_n |u_n(t)|$. An initial wave packet splits into two components traveling in opposite directions with the same group velocity. However, only the rightward-propagating component is amplified, a clear signature of the system's non-reciprocal behavior. The group velocity measured from the slope of the propagating wavefront is $v_g \approx 7.184$, which is in close agreement with the slope calculated from the dispersion relation shown in Fig. 1(b).

To quantify the one-way amplification, in Fig. 2(b), we show the temporal evolution of the logarithm of the instantaneous global maximum of the lattice displacement field, $\log(\|u(t)\|_\infty)$. The envelope of this logarithmic signal exhibits a linear trend, indicating exponential growth in the underlying displacement. A linear fit to the data yields a slope of approximately 0.71, representing the growth rate. This value closely matches the imaginary part of the complex dispersion relation, $\text{Im}[\omega(q^*)] \approx 0.70$, shown in Fig. 1(c).

Figure 2(c) shows the velocity time series for particles at positions $n = 130$ and $n = 160$, which are downstream from the excitation point. Both signals exhibit clear temporal amplification. The corresponding frequency spectra, presented in Fig. 2(d), reveal a dominant peak at $\omega \approx 24.38$. This value is consistent with the oscillation frequency, $\text{Re}[\omega(q^*)]$, from Fig. 1(b), where q^* is the wavenumber corresponding to the maximum growth rate.

In contrast, the velocity signals from upstream positions ($n = 49$ and $n = 3$), plotted in Fig. 2(e), show significant decay over time. The associated frequency spectra in Fig. 2(f) contain the same dominant frequency component, but its amplitude is substantially reduced. This confirms that while the initial disturbance propagates in both directions, non-reciprocity leads to strong wave amplification in the forward (downstream) direction and attenuation in the backward (upstream) direction.

Thus far, we have focused on systems with only elastic nonreciprocity. We now examine how the introduction of viscous damping influences this behavior. The simplest approach is to incorporate a damper in two ways: (i) onsite damping, which acts on the velocity of individual particles, and (ii) intersite damping, which depends on the relative velocity between neighboring particles. We discuss these cases sequentially in the following sections.

B. Onsite Damper

We now incorporate onsite damping into the lattice model, characterized by the damping coefficient c_g , as

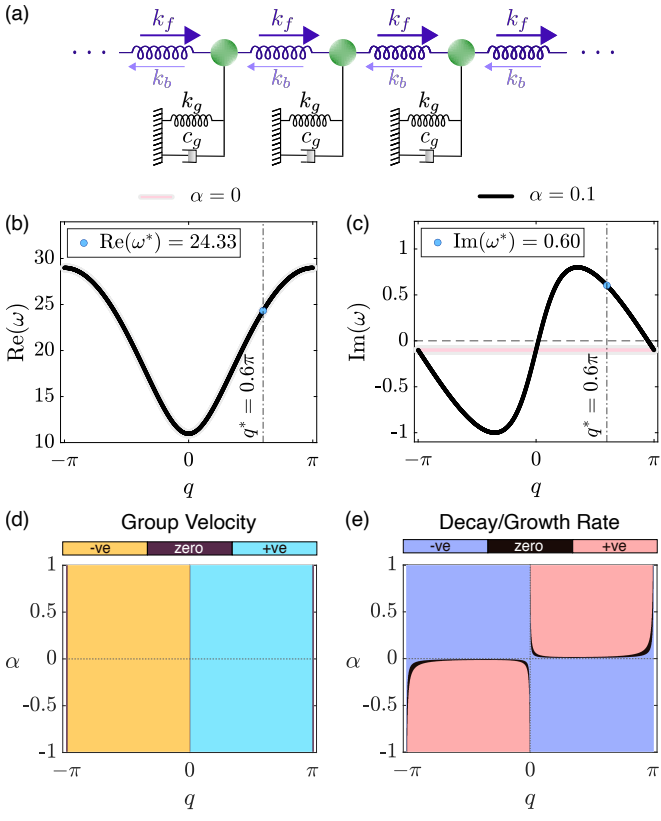


FIG. 3. Wave propagation in a 1D lattice with nonreciprocal stiffness and onsite damping. (a) Schematic of the lattice with asymmetric intersite springs and onsite viscous dampers; (b–c) Real and imaginary parts of the complex dispersion relation $\omega(q)$ for asymmetry parameters $\alpha = 0$ and $\alpha = 0.1$. (d–e) Parametric maps showing the signs of group velocity and temporal growth/decay rate as functions of q and α . We take onsite damping $c_g = 0.2$. Other parameters are the same as in Fig. 1.

shown in Fig. 3(a). The equation of motion becomes

$$m\ddot{u}_n + c_g\dot{u}_n + (2k + k_g)u_n - k(1 + \alpha)u_{n-1} - k(1 - \alpha)u_{n+1} = 0. \quad (7)$$

Applying the Bloch-Floquet ansatz yields the following dispersion relation:

$$\omega^2 + i\frac{c_g}{m}\omega - \frac{1}{m} \left[k_g + 2k(1 - \cos q) + 2ik\alpha \sin q \right] = 0. \quad (8)$$

Solving this quadratic equation for $\omega(q)$, we obtain

$$\omega(q) = -i\frac{c_g}{2m} + \sqrt{r(q)}e^{i\theta(q)/2}. \quad (9)$$

We select the root with the positive sign to ensure a positive oscillation frequency, corresponding to forward time evolution. Accordingly, the real and imaginary parts are

given by

$$\text{Re}[\omega(q)] = \sqrt{r(q)} \cos\left(\frac{\theta(q)}{2}\right), \quad (10)$$

$$\text{Im}[\omega(q)] = -\frac{c_g}{2m} + \sqrt{r(q)} \sin\left(\frac{\theta(q)}{2}\right), \quad (11)$$

where

$$\begin{aligned} r(q) &= \sqrt{A(q)^2 + B(q)^2}, \quad \theta(q) = \text{atan2}(B(q), A(q)), \\ A(q) &= -\left(\frac{c_g}{2m}\right)^2 + \frac{1}{m}[k_g + 2k(1 - \cos q)], \\ B(q) &= \frac{2k\alpha \sin q}{m}. \end{aligned}$$

The dispersion relation for this system is plotted in Figs. 3(b) and 3(c). For small non-reciprocity ($\alpha \sim \mathcal{O}(\epsilon)$) and damping ($c_g \sim \mathcal{O}(\epsilon)$), it can be approximated by

$$\begin{aligned} \text{Re}[\omega(q)] &= \sqrt{A_0(q)} + \frac{k^2 \alpha^2 \sin^2 q}{2m^2 A_0(q)^{3/2}} \\ &\quad - \frac{c_g^2}{8m^2 \sqrt{A_0(q)}} + \mathcal{O}(\epsilon^3), \end{aligned} \quad (12)$$

$$\text{Im}[\omega(q)] = \frac{k\alpha \sin q}{m\sqrt{A_0(q)}} - \frac{c_g}{2m} + \mathcal{O}(\epsilon^3), \quad (13)$$

where $A_0(q) = \frac{1}{m}[k_g + 2k(1 - \cos q)]$. In contrast to the case with no damper, the imaginary part of the frequency is uniformly shifted downward by $-c_g/(2m)$, as seen in Fig. 3(c). Furthermore, the higher-order correction to the real part is now negative, causing a *decrease* in the oscillation frequency, which is opposite to the behavior without a damper. While $\text{Re}[\omega(q)]$ remains a symmetric function of q , the constant negative shift renders $\text{Im}[\omega(q)]$ asymmetric.

The parametric plots in Figs. 3(d) and 3(e) illustrate the interplay between non-reciprocity and damping. While the sign of group velocity is largely unchanged, the boundaries in the growth/decay map are significantly altered, leading to a reduction in the parameter space for amplification. A notable feature is the existence of traveling waves ($\text{Im}[\omega(q)] = 0$) at wavenumbers away from $q = 0$ and $q = \pm\pi$. By setting Eq. (13) to zero in the long-wavelength limit ($q \rightarrow 0$), we can find the condition for these waves:

$$\alpha q \approx \frac{c_g}{2k} \sqrt{\frac{k_g}{m}}. \quad (14)$$

This hyperbolic relationship between α and q for neutrally stable traveling waves can be verified by the boundary line separating the gain and decay regions near the origin in Fig. 3(e).

We now examine the effect of onsite damping on the wave dynamics of a finite lattice, with the results presented in Fig. 4. The initial perturbation is a spatially localized Gaussian displacement near the center of the lattice, identical to the undamped case. While both forward and backward propagating waves are observed,

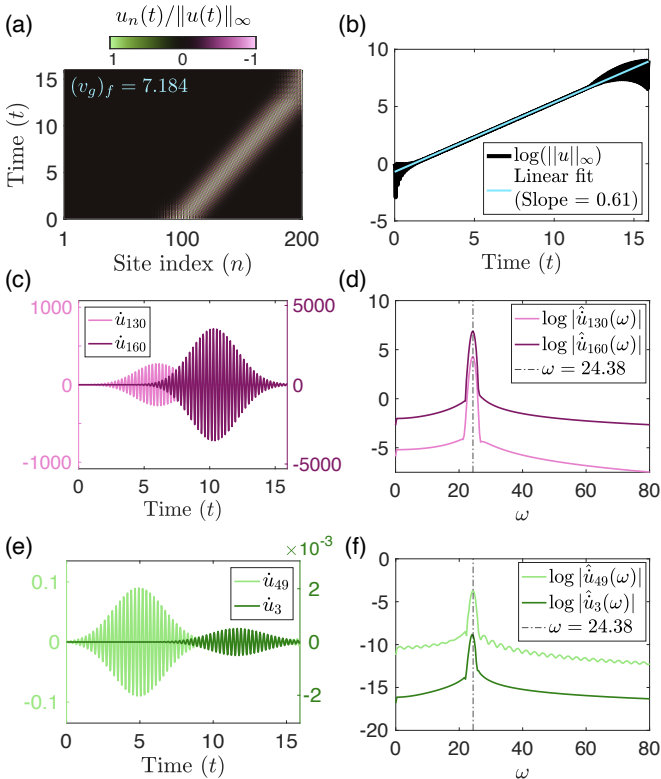


FIG. 4. Numerical demonstration of directional wave amplification in a 1D lattice with nonreciprocal stiffness and onsite damping. (a) Space-time evolution of the normalized displacement field, showing amplified wave propagation in the forward direction with a measured group velocity $v_g \approx 7.184$. (b) Logarithmic plot of the instantaneous global maximum, where a linear fit yields a slope of 0.61, indicating a reduced temporal growth rate due to the presence of onsite damping. (c–d) Velocity responses and corresponding spectral amplitudes at downstream sites ($n = 130, 160$) confirm energy amplification and dominant excitation near $\omega \approx 24.38$. (e–f) Upstream sites ($n = 49, 3$) show significant attenuation in both time and frequency domains, affirming unidirectional energy transport.

their amplitudes evolve differently due to the interplay between nonreciprocal stiffness and damping.

Figure 4(a) shows unidirectional wave propagation with a forward group velocity of $v_{g,f} \approx 7.18$, indicating that a small onsite damping does not significantly alter the wave speed. From Fig. 4(b), we measure a growth rate of 0.61, which confirms that the amplification persists, albeit at a reduced rate. The growth of velocity amplitudes at a downstream location, depicted in Figs. 4(c) and 4(d), further confirms this unidirectional amplification. This effect is weaker than in the undamped case; however, the spectral peak at $\omega \approx 24.38$ remains largely unaffected. Conversely, the backward-propagating signal shown in Figs. 4(e) and 4(f) is more strongly attenuated than its undamped counterpart, while its dominant frequency is unchanged. Overall, these findings demon-

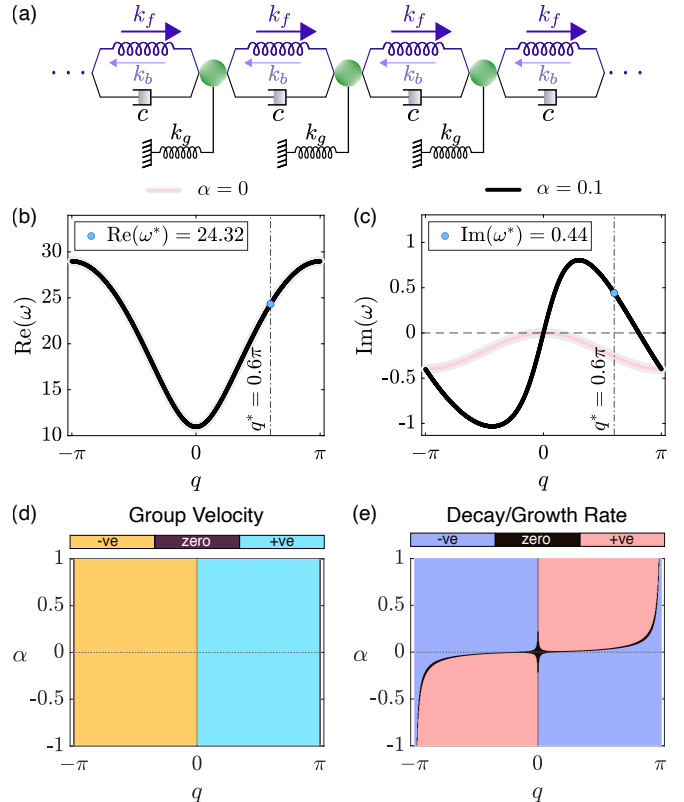


FIG. 5. Wave propagation in a 1D lattice with nonreciprocal stiffness and intersite damping. (a) Schematic of the lattice featuring direction-dependent springs and intersite viscous dampers. (b–c) Real and imaginary parts of the complex dispersion relation $\omega(q)$ for $\alpha = 0$ and $\alpha = 0.1$. (d–e) Parametric plots of the signs of group velocity and decay/growth rate as functions of q and α . We take $c = 0.2$, and keep other parameters the same as in Fig. 1.

strate that the nonreciprocal amplification mechanism survives in the presence of a small onsite damping.

C. Intersite Damper

We now introduce intersite damping into the lattice model, characterized by the damping coefficient c , as shown in Fig. 5(a). The equation of motion becomes

$$\begin{aligned} m\ddot{u}_n + c(2\dot{u}_n - \dot{u}_{n-1} - \dot{u}_{n+1}) + (2k + k_g)u_n \\ - k(1 + \alpha)u_{n-1} - k(1 - \alpha)u_{n+1} = 0. \end{aligned} \quad (15)$$

Applying the Bloch-Floquet ansatz yields the following dispersion relation:

$$\begin{aligned} \omega^2 + i\frac{2c(1 - \cos q)}{m}\omega \\ - \frac{1}{m}[k_g + 2k(1 - \cos q) + 2ik\alpha \sin q] = 0. \end{aligned} \quad (16)$$

Solving this quadratic equation for $\omega(q)$, we obtain

$$\omega(q) = -i\frac{c(1 - \cos q)}{m} + \sqrt{r(q)}e^{i\theta(q)/2}. \quad (17)$$

We select the root with the positive sign to ensure a positive oscillation frequency, corresponding to forward time evolution. Accordingly, the real and imaginary parts are given by

$$\text{Re}[\omega(q)] = \sqrt{r(q)} \cos\left(\frac{\theta(q)}{2}\right), \quad (18)$$

$$\text{Im}[\omega(q)] = -\frac{c}{m}(1 - \cos q) + \sqrt{r(q)} \sin\left(\frac{\theta(q)}{2}\right), \quad (19)$$

where

$$r(q) = \sqrt{A(q)^2 + B(q)^2}, \quad \theta(q) = \text{atan2}(B(q), A(q)),$$

$$A(q) = \frac{1}{m}[k_g + 2k(1 - \cos q)] - \frac{c^2}{m^2}(1 - \cos q)^2,$$

$$B(q) = \frac{2k\alpha}{m} \sin q.$$

The dispersion relation for this system is plotted in Figs. 5(b) and 5(c). For small non-reciprocity ($\alpha \sim \mathcal{O}(\epsilon)$) and damping ($c \sim \mathcal{O}(\epsilon)$), we approximate the dispersion relation as

$$\begin{aligned} \text{Re}[\omega(q)] &= \sqrt{A_0(q)} + \frac{k^2 \alpha^2 \sin^2 q}{2m^2 A_0(q)^{3/2}} \\ &\quad - \frac{c^2(1 - \cos q)^2}{2m^2 \sqrt{A_0(q)}} + \mathcal{O}(\epsilon^3), \end{aligned} \quad (20)$$

$$\text{Im}[\omega(q)] = \frac{k\alpha \sin q}{m\sqrt{A_0(q)}} - \frac{c(1 - \cos q)}{m} + \mathcal{O}(\epsilon^3), \quad (21)$$

where $A_0(q) = \frac{1}{m}[k_g + 2k(1 - \cos q)]$. In contrast to the uniform frequency shift from onsite damping, the imaginary part of the frequency in the intersite case is shifted downward by a wavenumber-dependent term, $-c(1 - \cos q)/m$. As shown in Fig. 5(c), this damping effect is zero at $q = 0$ and maximal at the edge of the Brillouin zone ($q = \pm\pi$). The higher-order correction to $\text{Re}[\omega(q)]$ due to damping is again negative, similar to the onsite case. Nevertheless, $\text{Re}[\omega(q)]$ still remains a symmetric function of q . However, the q -dependent shift results in a distinct asymmetric profile for $\text{Im}[\omega(q)]$.

We show the parametric plots in Figs. 5(d) and 5(e). While the group velocity characteristics remain largely unchanged, the boundaries separating gain and decay are qualitatively different from the onsite case. Notably, attenuation is now more pronounced near $q = \pm\pi$. Consequently, the condition for neutrally stable traveling waves ($\text{Im}[\omega] = 0$) is reshaped. By setting the imaginary part of the frequency from our approximation to zero in the long-wavelength limit ($q \rightarrow 0$), we find this condition to be

$$\alpha \approx \left(\frac{c}{2k}\sqrt{\frac{k_g}{m}}\right)q. \quad (22)$$

This linear relationship between α and q , in sharp contrast to the hyperbolic condition found for the onsite damper, can be verified by the boundary line near the origin in Fig. 5(f).

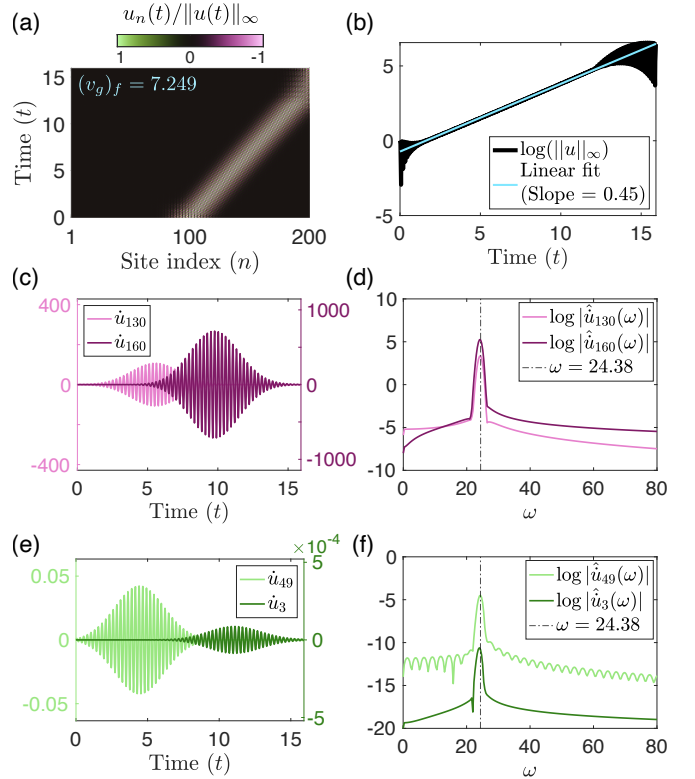


FIG. 6. Numerical demonstration of directional wave amplification in a 1D lattice with nonreciprocal stiffness and intersite damping. (a) Space-time colormap of the normalized displacement field, showing rightward amplification of the wave packet. The measured group velocity $v_g \approx 7.249$ agrees with the theoretical prediction. (b) Logarithmic plot of the instantaneous global maximum of the displacement field, with a linear fit showing a slope of 0.45, in close agreement with the analytical growth rate. (c–d) Velocity profiles and corresponding spectra at downstream sites ($n = 130, 160$) confirm energy amplification at the dominant frequency $\omega \approx 24.38$. (e–f) Upstream responses at ($n = 49, 3$) show strong attenuation in both time and frequency domains.

We next examine the effect of intersite damping on the wave dynamics of the finite lattice. The results, presented in Fig. 6, show that unidirectional amplification of a wave packet is preserved, similar to the case with onsite damping. While the group velocity is comparable, the amplification rate differs significantly. This is consistent with the asymmetry observed in the imaginary part of the frequency, $\text{Im}(\omega)$, as shown in the dispersion diagram [Fig. 5(c)]. These findings demonstrate that the nonreciprocal amplification mechanism survives in the presence of a small intersite damping, although the growth rate is altered differently than for onsite damping.

To summarize, we have investigated the role of damping in a lattice with nonreciprocal stiffness by considering three representative cases: no damping, onsite damping, and intersite damping. The incorporation of onsite damping reduces the amplification rate uniformly across

the wavenumber spectrum while preserving the directionality and coherence of the forward wave. In contrast, intersite damping introduces a wavenumber-dependent modification of the growth rates.

In the next section, we shift our focus to a distinct configuration involving a reciprocal elastic lattice equipped with a nonreciprocal intersite damper. This setup reverses the roles of stiffness and damping in imparting nonreciprocity, allowing us to isolate and study the wave manipulation capabilities arising purely from dissipative asymmetry.

III. LATTICE WITH NON-RECIPROCAL DAMPING

This section considers a system with reciprocal stiffness ($\alpha = 0$) and non-reciprocal intersite damping. The damping in the forward direction is taken to be $c_f = c(1+\beta)$, while in the backward direction it is $c_b = c(1-\beta)$, where $\beta \in [-1, 1]$. The governing equation of motion for this model, ignoring onsite damping, is

$$m\ddot{u}_n + c(2\dot{u}_n - (1+\beta)\dot{u}_{n-1} - (1-\beta)\dot{u}_{n+1}) + (2k + k_g)u_n - k(u_{n-1} + u_{n+1}) = 0. \quad (23)$$

The resulting dispersion relation can be expressed as

$$\omega(q) = \frac{c\beta}{m} \sin q - i \frac{c(1 - \cos q)}{m} + \sqrt{r(q)} e^{i\theta(q)/2}. \quad (24)$$

The real and imaginary parts are given by

$$\text{Re}[\omega(q)] = \frac{c\beta}{m} \sin q + \sqrt{r(q)} \cos\left(\frac{\theta(q)}{2}\right), \quad (25)$$

$$\text{Im}[\omega(q)] = -\frac{c}{m}(1 - \cos q) + \sqrt{r(q)} \sin\left(\frac{\theta(q)}{2}\right), \quad (26)$$

where

$$\begin{aligned} r(q) &= \sqrt{A(q)^2 + B(q)^2}, \quad \theta(q) = \text{atan2}(B(q), A(q)), \\ A(q) &= \frac{1}{m} [k_g + 2k(1 - \cos q)] + \frac{c^2\beta^2}{m^2} \sin^2 q \\ &\quad - \frac{c^2}{m^2}(1 - \cos q)^2, \\ B(q) &= -\frac{2c^2\beta}{m^2} \sin q(1 - \cos q). \end{aligned}$$

These results reveal a different non-reciprocal mechanism compared to the case of non-reciprocal springs. The presence of the term proportional to $\sin q$ in Eq. (25) makes the oscillation frequency $\text{Re}[\omega(q)]$ also asymmetric with respect to $q = 0$.

For small damping ($c \sim \mathcal{O}(\epsilon)$) and non-reciprocity ($\beta \sim \mathcal{O}(\epsilon)$), the approximate dispersion relations are:

$$\text{Re}[\omega(q)] = \sqrt{A_0(q)} - \frac{c^2(1 - \cos q)^2}{2m^2\sqrt{A_0(q)}} + \frac{c\beta}{m} \sin q + \mathcal{O}(\epsilon^3), \quad (27)$$

$$\text{Im}[\omega(q)] = -\frac{c}{m}(1 - \cos q) + \mathcal{O}(\epsilon^3), \quad (28)$$

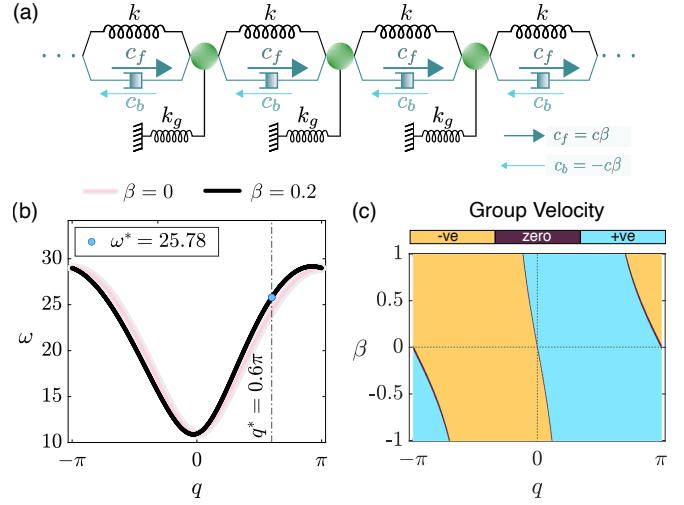


FIG. 7. Wave propagation in a 1D lattice with a gyroscopic damper. (a) Schematic of the lattice featuring gyroscopic damping, implemented via forward and backward dashpots with $c_f = c\beta$ and $c_b = -c\beta$, alongside reciprocal intersite stiffness k and onsite stiffness k_g . (b) Purely real dispersion relation $\omega(q)$ for $\beta = 0$ and $\beta = 0.2$. (c) Parametric plot showing the sign of the group velocity as a function of wavenumber q and damping asymmetry parameter β , revealing directional bias induced by the nonreciprocal damping configuration. We take $c = 7.5$ and keep other parameters the same.

where $A_0(q) = \frac{1}{m}[k_g + 2k(1 - \cos q)]$. The leading-order terms indicate that the real component has an asymmetric shift proportional to β , while the imaginary component is nearly symmetric but negative, implying that the wave will attenuate in both directions at approximately the same rate.

Special non-reciprocal damping: Gyroscopic damping

The preceding model exhibits both an asymmetric real dispersion relation and global wave decay. To isolate the frequency asymmetry from the dissipative effects, we now define a special non-reciprocal damper that leads to purely oscillatory dynamics. As depicted in Fig. 7(a), this corresponds to an effective damping of $c\beta$ in the forward direction and $-c\beta$ in the backward direction. This is akin to gyroscopic damping that is not dissipative (Attarzadeh *et al.*, 2019; Baz, 2020; Carta *et al.*, 2014; Wang *et al.*, 2015). This construction isolates the non-reciprocal behavior from the net dissipation inherent in standard intersite damping. In addition, this special case will later be combined with non-reciprocal stiffness to explore novel wave dynamics.

The governing equation of motion for a lattice with this gyroscopic damper is

$$m\ddot{u}_n + c\beta(\dot{u}_{n+1} - \dot{u}_{n-1}) + (2k + k_g)u_n - k(u_{n-1} + u_{n+1}) = 0, \quad (29)$$

and the associated dispersion relation is

$$\omega(q) = \frac{c\beta}{m} \sin q + \sqrt{\frac{c^2\beta^2}{m^2} \sin^2 q + \frac{1}{m} [k_g + 2k(1 - \cos q)]}. \quad (30)$$

The dispersion relation in Eq. (30) has two key features. First, the term $\sin q$ breaks the symmetry, $\omega(q) \neq \omega(-q)$. Second, the frequency $\omega(q)$ is purely real for all q , indicating that the system is free of any dissipation. This frequency asymmetry is illustrated in Fig. 7(b).

The group velocity consequently loses its symmetry as well. Figure 7(c) shows a parametric plot demonstrating that, in contrast to the case of non-reciprocal stiffness, points of zero group velocity can emerge at wavenumbers other than $q = 0$ or $q = \pm\pi$. Interestingly, a similar observation is made related to the modification of Brillouin zone boundaries in the context of non-reciprocal Willis monatomic lattices (Al Ba'ba'a, 2023).

In the limit of weak non-reciprocity (β), Eq. (30) can be approximated as

$$\omega(q) = \sqrt{A_0(q)} + \frac{c\beta}{m} \sin q + \mathcal{O}(\beta^2), \quad (31)$$

where $A_0(q) = \frac{1}{m}[k_g + 2k(1 - \cos q)]$. From this approximate form, we can determine the condition for zero group velocity in the long-wavelength limit ($q \rightarrow 0$). The locus of points where $v_g(q) = 0$ is given by

$$\beta \approx -\frac{\sqrt{mk}}{c\sqrt{k_g}}q. \quad (32)$$

This linear relationship is consistent with the region near the origin in the parametric plot shown in Fig. 7(c).

We numerically investigate the effect of the gyroscopic damper in a finite lattice, with the results presented in Fig. 8. The lattice is excited by a spatially localized Gaussian displacement near its center. The spatiotemporal evolution of the displacement field, $u_n(t)$, reveals that the initial wave packet splits into forward- and backward-propagating components [Fig. 8(a)]. However, these components now propagate with different group velocities, with the backward-propagating wave traveling faster than the forward one.

As predicted by the purely real dispersion relation [Eq. (30)], the system is stable and exhibits no exponential growth or decay. This stability is corroborated by the global displacement norm, which remains bounded throughout the simulation [Fig. 8(b)]. The velocity time series at two symmetric probe locations ($n = 40$ and $n = 160$), shown in Fig. 8(c), confirms the different arrival times and shows that the wave packets maintain comparable amplitudes. A key finding is the emergence of spectral asymmetry: the velocity spectra in Fig. 8(d) reveal distinct peak frequencies for the forward-propagating ($\omega \approx 25.75$) and backward-propagating ($\omega \approx 23.00$) waves. This direction-dependent frequency shift is a direct consequence of the asymmetric dispersion shown in Fig. 7(b).

These finite-lattice simulations, therefore, confirm that this gyroscopic damper introduces direction-

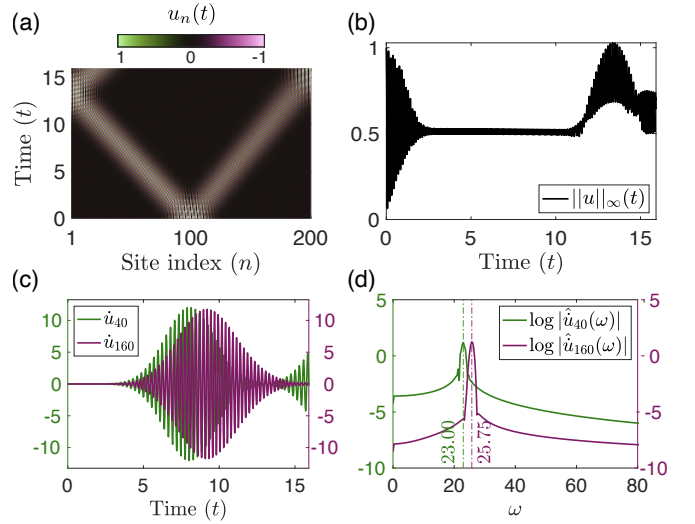


FIG. 8. **Numerical simulation of wave dynamics in a 1D lattice with gyroscopic damping.** (a) Space-time colormap of the displacement field $u_n(t)$ in a 200-particle finite lattice with fixed boundaries, illustrating symmetric wave amplitudes but asymmetric propagation speeds for left- and right-travelling wave packets. (b) Time evolution of the instantaneous global maximum, showing no net amplification or decay. (c–d) Velocity responses and their spectral amplitudes at sites $n = 40$ and 160 reveal the coexistence of two wave components with distinct group velocities, corresponding to slightly different peak frequencies ($\omega \approx 23.00$ and $\omega \approx 25.75$).

dependent group velocities and frequency shifts without inducing exponential amplification or attenuation.

We now advance to studying a lattice system where both nonreciprocal stiffness and gyroscopic damping act simultaneously. The previous sections highlighted how each mechanism individually breaks reciprocity—nonreciprocal stiffness enabled directional amplification via complex frequencies, while the gyroscopic damper induced frequency asymmetry without introducing net gain or loss. Their combined action is expected to produce richer, more intricate wave dynamics, shaped by both directional amplification and asymmetric group velocities. In the following section, we investigate this interplay and its implications on dispersion, enhanced directional decay or growth, and wave transport in the lattice.

IV. LATTICE WITH COMBINED NON-RECIPROCAL STIFFNESS AND DAMPING

We now analyze a system that combines nonreciprocal intersite stiffness (governed by α) with a gyroscopic damper (governed by β). This configuration enables a rich interplay between directional amplification due to stiffness asymmetry and oscillation frequency asymmetry introduced by non-reciprocal damping. As illustrated in Fig. 9(a), each mass in the lattice is connected to its

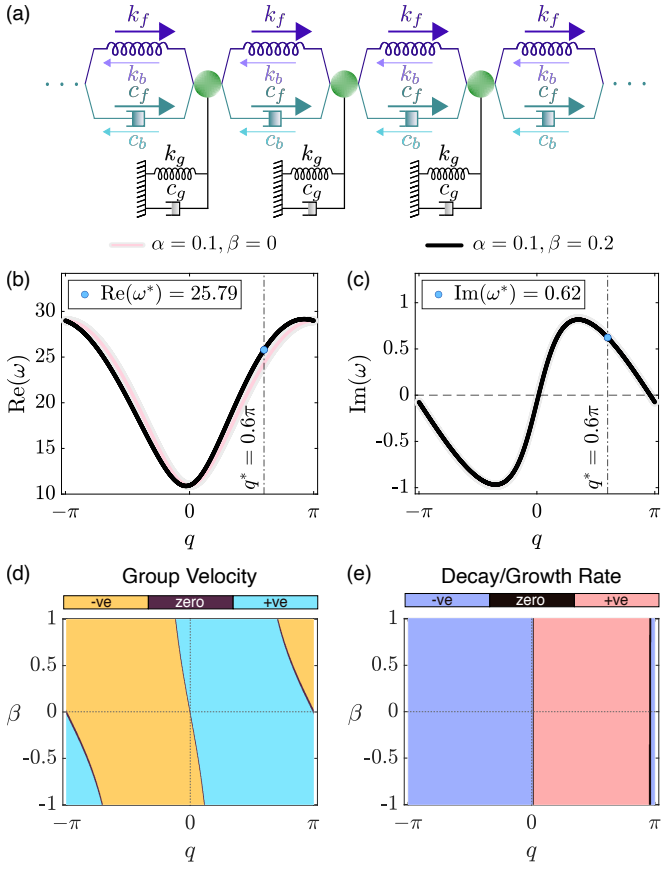


FIG. 9. Wave propagation in a 1D lattice with combined nonreciprocal stiffness and damping. (a) Lattice with unit cell featuring both asymmetric springs ($k_f = k(1+\alpha)$, $k_b = k(1-\alpha)$) and gyroscopic dampers ($c_f = c\beta$, $c_b = -c\beta$), along with onsite stiffness k_g and damping c_g . (b–c) Real and imaginary parts of the complex dispersion relation $\omega(q)$ for $\beta = 0$ and $\beta = 0.2$ at a fixed $\alpha = 0.1$. (d–e) Parametric maps of the group velocity and temporal growth/decay rate versus q and β , demonstrating pronounced direction-dependent transport. We take $c = 7.5$ and $c_g = 0.3$. All other parameters are consistent with previous cases.

neighbors via asymmetric springs with $k_f = k(1 + \alpha)$, $k_b = k(1 - \alpha)$, and nonreciprocal dampers with $c_f = c\beta$, $c_b = -c\beta$. Additionally, onsite stiffness k_g and damping c_g anchor each mass to ground.

The governing equation of motion for the n th mass in the lattice reads:

$$m\ddot{u}_n + c_g\dot{u}_n + c\beta(\dot{u}_{n+1} - \dot{u}_{n-1}) + (2k + k_g)u_n - k(1 + \alpha)u_{n-1} - k(1 - \alpha)u_{n+1} = 0. \quad (33)$$

The corresponding characteristic equation yields the exact dispersion relation:

$$\omega(q) = -i\frac{c_g}{2m} + \frac{c\beta}{m} \sin q + \sqrt{r(q)} e^{i\theta(q)/2}, \quad (34)$$

with the real and imaginary parts given by

$$\text{Re}[\omega(q)] = \frac{c\beta}{m} \sin q + \sqrt{r(q)} \cos\left(\frac{\theta(q)}{2}\right), \quad (35)$$

$$\text{Im}[\omega(q)] = -\frac{c_g}{2m} + \sqrt{r(q)} \sin\left(\frac{\theta(q)}{2}\right), \quad (36)$$

where

$$r(q) = \sqrt{A(q)^2 + B(q)^2}, \quad \theta(q) = \text{atan2}(B(q), A(q)), \\ A(q) = \frac{1}{m} [k_g + 2k(1 - \cos q)] + \frac{c^2\beta^2}{m^2} \sin^2 q - \frac{c_g^2}{4m^2}, \\ B(q) = \frac{2k\alpha}{m} \sin q - \frac{c_g c \beta \sin q}{m^2}.$$

For small values of α , β , and c_g (i.e., $\sim \mathcal{O}(\epsilon)$), a first-order Taylor expansion provides additional insight:

$$\text{Re}[\omega(q)] = \sqrt{A_0(q)} + \frac{c\beta}{m} \sin q + \mathcal{O}(\epsilon^2) \quad (37)$$

$$\text{Im}[\omega(q)] = \frac{k\alpha \sin q}{m\sqrt{A_0(q)}} - \frac{c_g}{2m} + \mathcal{O}(\epsilon^2), \quad (38)$$

where $A_0(q) = \frac{1}{m}[k_g + 2k(1 - \cos q)]$.

These results reveal a remarkable decoupling of the two non-reciprocal effects at leading order. The imaginary part of the frequency, which governs temporal growth or decay, is determined entirely by the non-reciprocal stiffness parameter α , and matches the expression for lattice with nonreciprocal stiffness and onsite damping. The real part, on the other hand, acquires an asymmetric contribution from the non-reciprocal damper β , inducing a direction-dependent frequency shift without altering the system's gain or loss characteristics. This enables independent tuning of wave amplification and oscillation frequency through parameters α and β , respectively.

Figures 9(b) and 9(c) present the real and imaginary parts of the complex dispersion relation, $\omega(q)$, for a fixed stiffness asymmetry ($\alpha = 0.1$) to investigate the influence of the parameter β . While the imaginary part, $\text{Im}[\omega(q)]$, is nearly identical to the case where $\beta = 0$, the real part, $\text{Re}[\omega(q)]$, becomes asymmetric for non-zero values of β .

This behavior is further detailed in the parametric maps shown in Figs. 9(d) and 9(e). The group velocity map [Fig. 9(d)] exhibits a strong asymmetry in both sign and magnitude that is tunable by β . In contrast, the growth rate map [Fig. 9(e)] confirms that $\text{Im}[\omega(q)]$ is largely insensitive to β . The inherent asymmetry in the growth rate with respect to the wavenumber q is therefore preserved, as it is governed by the nonreciprocal stiffness α .

We present finite chain simulations in Fig. 10 to investigate the interplay between nonreciprocal stiffness and nonreciprocal damping. The simulations are performed for two contrasting cases of the damping parameter, $\beta = -0.2$ and $\beta = +0.2$, while the stiffness asymmetry is held constant at $\alpha = 0.1$. As in previous sections, the system is excited by a Gaussian-modulated initial displacement at its center.

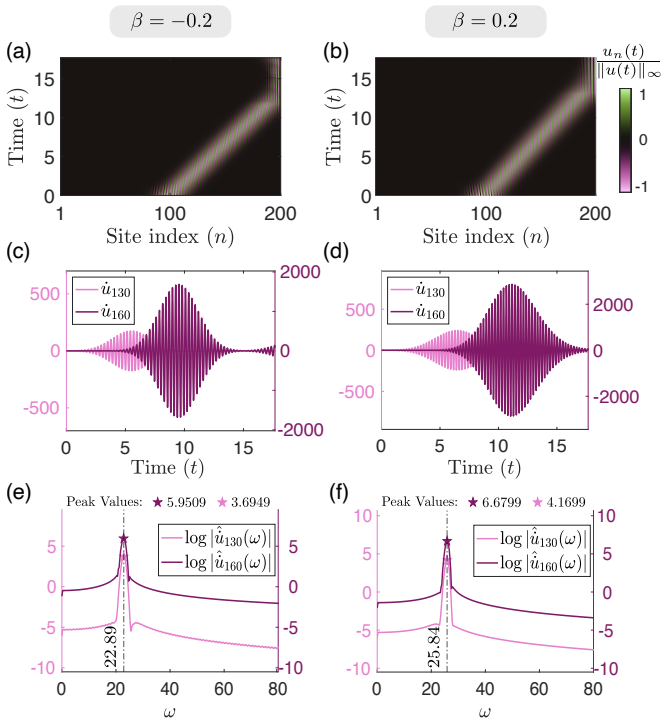


FIG. 10. Finite lattice simulation illustrating amplification dependence on β in a system with combined nonreciprocal stiffness and gyroscopic damping. (a,b) Space–time plots of normalized displacement for $\beta = \pm 0.2$. (c,d) Corresponding time-domain velocity responses at $n = 130, 160$. The case with $\beta = 0.2$ shows a slightly more amplified wavepacket due to slower group velocity. (e,f) Velocity spectra reveal dominant frequencies. We take $\alpha = 0.1$ and keep other parameters the same as before.

The results reveal that the sign of β provides a mechanism to control wave dynamics. Figures 10(a) and 10(b) show that the forward-propagating wave is amplified in both cases, a characteristic governed by the nonreciprocal stiffness α . However, switching the sign of β alters the group velocity of the wave packet. This is explicitly confirmed by the velocity time series at downstream sites ($n = 130$ and $n = 160$) in Figs. 10(c) and (d), which show that the wave packet for $\beta = -0.2$ arrives at a given site faster than for $\beta = +0.2$.

Interestingly, while the amplification rate is set by α , the net amplification at a specific site depends on the group velocity as well. For $\beta = +0.2$, the wave packet travels slower, allowing more time for the amplification, resulting in a larger amplitude at a given location compared to the $\beta = -0.2$ case. The net amplification is therefore a combined effect of the growth rate (dictated by α) and the propagation time (dictated by β). This is one of the key results of our work.

Finally, Figs. 10(e) and 10(f) show that the sign of β also shifts the dominant frequency of the amplified wave, along with a gain in the spectral content. This tunability is further explored in Fig. 11, which plots the

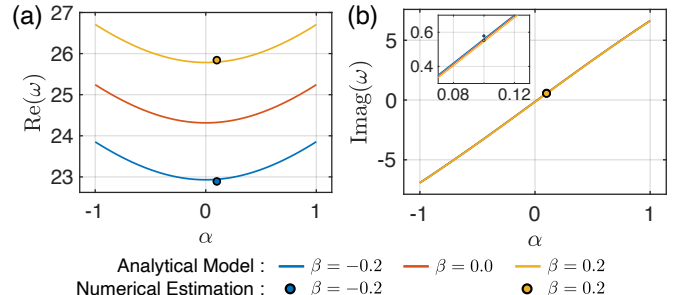


FIG. 11. Effect of α and β on dominant oscillation frequency and temporal growth at $q = 0.6\pi$. (a) Real part of the dominant eigenfrequency $\text{Re}(\omega)$ plotted as a function of stiffness asymmetry α for $\beta = -0.2, 0, 0.2$. Change in β leads to a significant change in oscillation frequency for a fixed α . (b) Imaginary part $\text{Im}(\omega)$ for the same parameter sweep shows minimal variation, suggesting that damping asymmetry has a negligible effect on the temporal growth rate. Solid lines represent analytical results from the complex dispersion relation, and circular markers indicate numerically extracted peak frequencies from finite-lattice simulations (see Fig. 10). The inset in (b) confirms close agreement between analytical and numerical growth rates at $\alpha = 0.1$.

dominant amplified frequency as a function of α and β for a forward-propagating wave. The frequency exhibits a nearly quadratic dependence on α for a fixed β [Fig. 11(a)], consistent with the higher-order corrections in Eq. (12). In contrast, Fig. 11(b) demonstrates that varying β provides an effective route to tune the wave's frequency while leaving the amplification rate, governed by α , nearly unchanged.

In summary, while the amplification rate of waves is primarily determined by α , the sign and magnitude of β can be used to tune net amplification (through changing the group velocity) and the dominant frequency of the wave packet.

Wave mixing through boundary reflection

In a finite system, boundaries are not merely passive reflectors but can be actively utilized to manipulate wave properties. Here, we investigate how boundary reflection can induce “wave mixing”, providing an additional mechanism for tuning the amplified signal’s frequency content. We achieve this by launching a wave packet near one end of the lattice. The backward-propagating (attenuated) component travels to the opposite boundary, reflects, and then propagates forward, mixing with the original forward-propagating (amplified) component. As we will show, the nonreciprocal damping parameter β is crucial in controlling the effectiveness of this mixing. Figure 12 compares the dynamics for $\beta = -0.2$ (left column) and $\beta = +0.2$ (right column), keeping the stiffness asymmetry fixed at $\alpha = 0.1$.

The ray diagram in Figs. 12(a) and 12(b) illustrate this process. The backward-propagating wave has a sig-

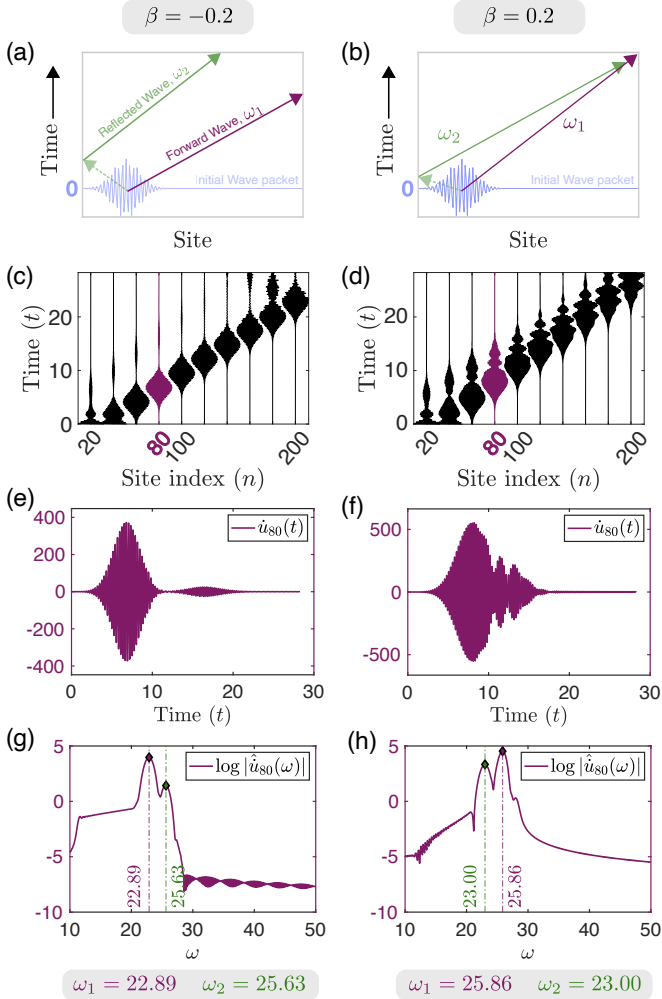


FIG. 12. Effect of boundaries on wave mixing and amplification for $|q^*| = 0.6\pi$. (a,b) Ray diagram for the evolution of the initial wave packet placed near the left boundary. Backward traveling wave has a different group velocity, and then it reflects to mix with the forward amplifying wave. (c,d) Spatiotemporal velocity waterfall plots, illustrating wave propagation and boundary interactions as one changes β . The backward-propagating wave reflects off the left boundary and re-enters the lattice, leading to additional interaction with the medium. (e,f) Velocity response at site 80 captures both the initial forward-propagating wave and the subsequent reflected wave packet. (g,h) Frequency spectra at site 80 display two distinct peaks associated with the forward and reflected modes but in different relative amplitudes.

nificantly faster group velocity for $\beta = +0.2$ compared to $\beta = -0.2$. Consequently, it reaches the boundary and reflects more quickly, experiencing less attenuation during its transit. This difference in travel time and attenuation directly impacts the local dynamics, as seen in the velocity waterfall plots in Figs. 12(c) and 12(d). When we extract velocity time series at site $n = 80$ [Figs. 12(e) and 12(f)] for these cases, the difference is clear. For

$\beta = -0.2$, the slower backward wave is heavily attenuated, resulting in a reflected packet that is well-separated in time and has a modest amplitude. For $\beta = +0.2$, the faster, less-attenuated backward wave produces a much stronger reflected packet that arrives sooner, enabling a more effective mixing of the two components.

The consequence of this wave mixing is evident in the frequency spectra of the signal at site $n = 80$, shown in Figs. 12(g) and 12(h). Recall that the forward and backward waves have different dominant frequencies. For $\beta = +0.2$, the effective mixing of the strong reflected wave with the forward wave results in a spectrum where two distinct frequency peaks, $\omega \approx 25.86$ (forward wave) and $\omega \approx 23.00$ (reflected wave) are prominent and significantly amplified. In contrast, for $\beta = -0.2$, the spectrum is dominated by the forward wave ($\omega \approx 22.89$) and reflected wave ($\omega \approx 25.63$), but the weak reflection has a smaller impact. The value of β along with the boundary thus acts as a switch, controlling which frequencies are mixed and their relative dominance. Therefore, these results demonstrate that boundaries in nonreciprocal lattices can be seen as functional elements that enable complex wave-shaping phenomena in addition to wave amplification.

V. CONCLUSION

This work presents a comprehensive framework for controlling wave propagation in one-dimensional lattices by combining nonreciprocal stiffness and engineered damping. We first established that conventional onsite and intersite viscous damping mechanisms, while modifying the system's dispersion, primarily counteract the gain from nonreciprocal stiffness, thereby offering limited control over wave propagation. In contrast, by introducing a non-dissipative gyroscopic damping mechanism, we uncovered our central result: a robust decoupling of control. This allows the nonreciprocal stiffness (α) to dictate the temporal growth rate, while the gyroscopic damping (β) independently tunes the wave's group velocity and oscillation frequency.

This decoupling of temporal gain from wave kinematics enables novel phenomena. By tuning β , the travel time of a wave packet through the amplifying medium can be controlled, leading to the key insight that slower-propagating waves accumulate greater net amplification due to prolonged exposure to the gain mechanism. Furthermore, we demonstrated that boundaries in finite systems can be functionalized to induce wave mixing. The parameter β governs the efficacy of this mixing by controlling the transit time and attenuation of reflected waves, thereby enabling the selective amplification of distinct frequency components. These behaviors, predicted by our analytical models, were consistently validated by time-domain simulations.

These findings provide a versatile toolkit for programming wave behavior, with significant implications for the design of active metamaterials. The ability to independently manage gain, group velocity, and fre-

quency offers a new paradigm for engineering systems with on-demand functionalities, including advanced unidirectional amplifiers, reconfigurable vibration isolators, and acoustic diodes.

Future research could explore experimental realization of this model, potentially through active electronic circuits or feedback-controlled mechanical systems. A compelling direction exploration of topological features and bulk-boundary correspondence in these lattices and their extension to higher dimensions. Finally, investigating the influence of disorder, nonlocality (Rosa and Ruzzene, 2020), and nonlinearity (Veenstra *et al.*, 2024) on these systems remains a rich area for exploration, promising to uncover more complex spatiotemporal wave dynamics.

ACKNOWLEDGMENTS

We thank Prof. Nicholas Boechler and Prof. Nicholas Gravish of the University of California, San Diego, for insightful discussions. R.C. gratefully acknowledges support from the Indian Institute of Science Startup Grant.

- Al Ba'b'a, H. B. (2023). “Brillouin-zone definition in nonreciprocal willis monatomic lattices,” *JASA Express Letters* **3**, 120001, doi.org/10.1121/10.0022535.
- Attarzadeh, M. A., Maleki, S., Crassidis, J. L., and Nouh, M. (2019). “Non-reciprocal wave phenomena in energy self-reliant gyric metamaterials,” *The Journal of the Acoustical Society of America* **146**(1), 789–801, doi.org/10.1121/1.5114916.
- Banerjee, D., Vitelli, V., Jülicher, F., and Surówka, P. (2021). “Active viscoelasticity of odd materials,” *Phys. Rev. Lett.* **126**, 138001, link.aps.org/doi/10.1103/PhysRevLett.126.138001.
- Baz, A. (2020). “Active synthesis of a gyroscopic-nonreciprocal acoustic metamaterial,” *The Journal of the Acoustical Society of America* **148**(3), 1271–1288, doi.org/10.1121/10.0001815.
- Brandenbourger, M., Locsin, X., Lerner, E., and Coulais, C. (2019). “Non-reciprocal robotic metamaterials,” *Nature Communications* **10**(1), 4608, doi.org/10.1038/s41467-019-12599-3.
- Carta, G., Brun, M., Movchan, A., Movchan, N., and Jones, I. (2014). “Dispersion properties of vortex-type monatomic lattices,” *International Journal of Solids and Structures* **51**(11), 2213–2225, www.sciencedirect.com/science/article/pii/S0020768314000742.
- Chen, Y., Li, X., Scheibner, C., Vitelli, V., and Huang, G. (2021). “Realization of active metamaterials with odd micropolar elasticity,” *Nature Communications* **12**, 5935, doi.org/10.1038/s41467-021-26034-z.
- Ding, K., Fang, C., and Ma, G. (2022). “Non-hermitian topology and exceptional-point geometries,” *Nature Reviews Physics* **4**, 745–760, www.nature.com/articles/s42254-022-00516-5.
- Gao, P., Qu, Y., and Christensen, J. (2022). “Non-hermitian elastodynamics in gyro-odd continuum media,” *Communications Materials* **3**, 74, doi.org/10.1038/s43246-022-00297-5.
- Ghatak, A., Brandenbourger, M., van Wezel, J., and Coulais, C. (2020). “Observation of non-hermitian topology and its bulk-edge correspondence in an active mechanical metamaterial,” *Proceedings of the National Academy of Sciences* **117**, 29561–29568, doi.org/10.1073/pnas.2010580117.
- Hatano, N., and Nelson, D. R. (1996). “Localization transitions in non-hermitian quantum mechanics,” *Phys. Rev. Lett.* **77**, 570–573, link.aps.org/doi/10.1103/PhysRevLett.77.570.

- Hatano, N., and Nelson, D. R. (1998). “Non-hermitian delocalization and eigenfunctions,” *Phys. Rev. B* **58**, 8384–8390, link.aps.org/doi/10.1103/PhysRevB.58.8384.
- Jana, S., Manda, B. M., Achilleos, V., Frantzeskakis, D. J., and Sirota, L. (2025). “Harnessing nonlinearity to tame wave dynamics in nonreciprocal active systems” arxiv.org/abs/2502.16216.
- Lin, R., Tai, T., Li, L., and Lee, C. H. (2023). “Topological non-hermitian skin effect,” *Frontiers of Physics* **18**(5), 53605, doi.org/10.1007/s11467-023-1309-z.
- Liu, S., Shao, R., Ma, S., Zhang, L., You, O., Wu, H., Xiang, Y. J., Cui, T. J., and Zhang, S. (2021). “Non-hermitian skin effect in a non-hermitian electrical circuit,” *Research* **2021**, spj.science.org/doi/abs/10.34133/2021/5608038.
- Maddi, A., Auregan, Y., Penelet, G., Pagneux, V., and Achilleos, V. (2024). “Exact analog of the hatano-nelson model in one-dimensional continuous nonreciprocal systems,” *Phys. Rev. Res.* **6**, L012061, link.aps.org/doi/10.1103/PhysRevResearch.6.L012061.
- Nassar, H., Yousefzadeh, B., Fleury, R., Ruzzene, M., Alù, A., Daraio, C., Norris, A. N., Huang, G., and Haberman, M. R. (2020). “Nonreciprocity in acoustic and elastic materials,” *Nature Reviews Materials* **5**(9), 667–685, doi.org/10.1038/s41578-020-0206-0.
- Rosa, M. I., and Ruzzene, M. (2020). “Dynamics and topology of non-hermitian elastic lattices with non-local feedback control interactions,” *New journal of physics* **22**(5), 053004, iopscience.iop.org/article/10.1088/1367-2630/ab81b6.
- Scheibner, C., Souslov, A., Banerjee, D., Surówka, P., Irvine, W. T. M., and Vitelli, V. (2020). “Odd elasticity,” *Nature Physics* **16**, 475–480, doi.org/10.1038/s41567-020-0795-y.
- Shen, H., Zhen, B., and Fu, L. (2018). “Topological band theory for non-hermitian hamiltonians,” *Phys. Rev. Lett.* **120**, 146402, link.aps.org/doi/10.1103/PhysRevLett.120.146402.
- Veenstra, J., Gamayun, O., Guo, X., Sarvi, A., Meinersen, C. V., and Coulais, C. (2024). “Non-reciprocal topological solitons in active metamaterials,” *Nature* **627**, 528–533, doi.org/10.1038/s41586-024-07097-6.
- Wang, P., Lu, L., and Bertoldi, K. (2015). “Topological phononic crystals with one-way elastic edge waves,” *Phys. Rev. Lett.* **115**, 104302, link.aps.org/doi/10.1103/PhysRevLett.115.104302.
- Wang, W., Wang, X., and Ma, G. (2022). “Non-hermitian morphing of topological modes,” *Nature* **608**(7921), 50–55, doi.org/10.1038/s41586-022-04929-1.
- Yao, S., and Wang, Z. (2018). “Edge states and topological invariants of non-hermitian systems,” *Phys. Rev. Lett.* **121**, 086803, link.aps.org/doi/10.1103/PhysRevLett.121.086803.
- Zhang, L., Yang, Y., Ge, Y., Guan, Y.-J., Chen, Q., Yan, Q., Chen, F., Xi, R., Li, Y., Jia, D., Yuan, S.-Q., Sun, H.-X., Chen, H., and Zhang, B. (2021). “Acoustic non-hermitian skin effect from twisted winding topology,” *Nature Communications* **12**(1), 6297, doi.org/10.1038/s41467-021-26619-8.
- Zhao, Y., Zhou, X., and Huang, G. (2020). “Non-reciprocal rayleigh waves in elastic gyroscopic medium,” *Journal of the Mechanics and Physics of Solids* **143**, 104065, www.sciencedirect.com/science/article/pii/S0022509620302994.

